



**HAL**  
open science

## Rapid directivity detection by azimuthal amplitude spectra inversion

Simone Cesca, Sebastian Heimann, Torsten Dahm

► **To cite this version:**

Simone Cesca, Sebastian Heimann, Torsten Dahm. Rapid directivity detection by azimuthal amplitude spectra inversion. *Journal of Seismology*, 2010, 15 (1), pp.147-164. 10.1007/s10950-010-9217-4 . hal-00642936

**HAL Id: hal-00642936**

**<https://hal.science/hal-00642936v1>**

Submitted on 20 Nov 2011

**HAL** is a multi-disciplinary open access archive for the deposit and dissemination of scientific research documents, whether they are published or not. The documents may come from teaching and research institutions in France or abroad, or from public or private research centers.

L'archive ouverte pluridisciplinaire **HAL**, est destinée au dépôt et à la diffusion de documents scientifiques de niveau recherche, publiés ou non, émanant des établissements d'enseignement et de recherche français ou étrangers, des laboratoires publics ou privés.

# Rapid directivity detection by azimuthal amplitude spectra inversion

Simone Cesca · Sebastian Heimann ·  
Torsten Dahm

Received: 24 February 2010 / Accepted: 4 November 2010  
© Springer Science+Business Media B.V. 2010

**1 Abstract** An early detection of the presence of  
2 rupture directivity plays a major role in the correct  
3 estimation of ground motions and risks associated  
4 to the earthquake occurrence. We present here  
5 a simple method for a fast detection of rupture  
6 directivity, which may be additionally used to  
7 discriminate fault and auxiliary planes and have  
8 first estimations of important kinematic source  
9 parameters, such as rupture length and rupture  
10 time. Our method is based on the inversion of  
11 amplitude spectra from P-wave seismograms to  
12 derive the apparent duration at each station and  
13 on the successive modelling of its azimuthal be-  
14 haviour. Synthetic waveforms are built assuming a  
15 spatial point source approximation, and the finite  
16 apparent duration of the spatial point source is  
17 interpreted in terms of rupture directivity. Since  
18 synthetic seismograms for a point source are cal-  
19 culated very quickly, the presence of directivity  
20 may be detected within few seconds, once a focal  
21 mechanism has been derived. The method is here  
22 first tested using synthetic datasets, both for lin-  
23 ear and planar sources, and then successfully ap-  
24 plied to recent Mw 6.2–6.8 shallow earthquakes in  
25 Peloponnese, Greece. The method is suitable for

automated application and may be used to im- 26  
prove kinematic waveform modelling approaches. 27  
28

**Keywords** Directivity · Earthquake source · 29  
Kinematic model · Amplitude spectra 30

## 1 Introduction 31

Tectonically driven shallow earthquake sources 32  
are generally explained by means of shear cracks 33  
occurring along a limited, almost planar region, 34  
we refer as the focal region. A point source repre- 35  
sentation is a common first approximation, which 36  
is valid when treating far-field low frequency seis- 37  
mic waveform, using wavelengths larger than the 38  
rupture size. Higher frequencies seismograms and 39  
spectra contain information which can be related 40  
to the finiteness of the rupture process and thus 41  
can be used to determine parameters describing 42  
the finite source. Size and shape of the rupture 43  
area, rupture velocity and preferential rupture 44  
directions, an effect known as rupture directivity, 45  
are some of the parameters which can be retrieved 46  
by the analysis of high-frequency waveforms. In 47  
particular, we are interested here in discussing the 48  
problem of early detection of rupture directiv- 49  
ity, distinguishing between a prominent or partial 50  
unilateral rupture (a case which will be further 51  
referred as asymmetric bilateral rupture), and a 52

S. Cesca (✉) · S. Heimann · T. Dahm  
Institut für Geophysik, Universität Hamburg,  
Bundesstrasse 55, 20146 Hamburg, Germany  
e-mail: simone.cesca@zmaw.de

53 bilateral one, with rupture nucleating at the centre  
54 of the rupture area and propagating toward its  
55 edges. The azimuthal dependency of amplitudes  
56 and durations of different seismic phases is a first  
57 indicator of directivity effects and is consequence  
58 of the characteristics of the finite rupture process  
59 along the fault plane, specifically the main di-  
60 rection and speed of the rupture front propaga-  
61 tion. Directivity has been often observed and has  
62 been modelled for several earthquakes in the past,  
63 with several studies treating specific earthquakes  
64 or limited datasets (e. g., McGuire et al. 2002;  
65 Warren and Shearer 2006; Caldeira et al. 2009). A  
66 quick detection of directivity effects is important  
67 towards a correct estimation of ground motions,  
68 stress field perturbations and tsunamogenic risks  
69 and consequently to mitigate earthquake effects.  
70 These considerations provide important reasons  
71 to further investigate and develop specific tools  
72 for stable, rapid and automated directivity de-  
73 tection, which can be used within early warning  
74 systems.

75 Several methods have been applied in the past  
76 to detect and classify earthquake source direc-  
77 tivity. A common approach is the identification  
78 of predominant unilateral ruptures from the time  
79 duration and spectral analysis of body wave pulses  
80 (e.g. Boore and Joyner 1978; Beck et al. 1995;  
81 Warren and Shearer 2006; Caldeira et al. 2009).  
82 Pulse lengths at different stations are interpreted  
83 in terms of the apparent duration of the source  
84 time function (STF), and their variation in depen-  
85 dence on azimuth and incidence angle is inter-  
86 preted to detect directivity: similarly to a Doppler  
87 effect in classical physics, shorter STFs would in-  
88 dicate a rupture propagating towards the consid-  
89 ered station, while longer pulses indicate a rupture  
90 propagation in the opposite direction. Directiv-  
91 ity effects may also be revealed based on the  
92 analysis of surface waves at different azimuths  
93 (Ben-Menahem 1961; Pro et al. 2007). Whereas  
94 time domain methods remain more common, a  
95 significant contribution within this type of inver-  
96 sion methods was provided by the spectral ap-  
97 proach discussed in Warren and Shearer (2006).  
98 This method is based on the spectral estimation  
99 of the pulse broadening and accounts for the az-  
100 imuthal and incidence angle dependencies; it is  
101 well suited for the analysis of intermediate and

102 deep focus earthquakes and was successfully ap-  
103 plied to several events. The main limits of this  
104 class of methods are related to the fact that wave  
105 propagation and the superposition of different  
106 seismic phases are not accounted, since wave  
107 propagation effects between source and receiver  
108 (Green's functions) are limited to the estimation  
109 of the incidence angle of given seismic phases.  
110 Another possible limitation is the requirement of  
111 several stations with good azimuthal coverage in  
112 order to ensure reliable results. A second range  
113 of applications, which on the contrary accounts  
114 precisely for the effects of the earth's model on  
115 the observed waveforms, is based on empirical  
116 Green's functions technique (Hartzell 1978; Li  
117 and Toksöz 1993; Velasco et al. 1994; Cassidy  
118 1995; Müller 1985; Velasco et al. 2004; Vallée  
119 2007). In this case, an aftershock with common  
120 hypocenter and focal mechanism of the studied  
121 event can be used to remove path effects, and iso-  
122 late finite source apparent durations at different  
123 stations. Evidently, the application of these tech-  
124 niques is strongly limited by the availability of  
125 a proper aftershock. Brüstle and Müller (1987),  
126 and Imanishi and Takeo (2002) have investigated  
127 the adoption of master-event techniques to detect  
128 directivity: the identification of stopping phases  
129 (Madariaga 1977, 1983; Bernard and Madariaga  
130 1984; Spudich and Frazer 1984) at different sta-  
131 tions was used there to determine the main di-  
132 rection of rupture propagation, besides other  
133 source properties. Stopping phases identification  
134 (Imanishi and Takeo 1998, 2002) typically re-  
135 quires a careful waveform analysis, which may be  
136 hardly implemented within automated routines.  
137 A third group of techniques are based on com-  
138 plete kinematic waveform inversion, with the aim  
139 of retrieving a most detailed image of the finite  
140 rupture process, not limited to the identification  
141 of directivity. The range of methods and appli-  
142 cations is very wide, including higher order mo-  
143 ment tensor analysis (Dahm and Krüger 1999;  
144 McGuire et al. 2001, 2002), detailed slip map  
145 approaches (e.g. Olson and Apsel 1982; Hartzell  
146 and Helmberger 1982; Hartzell and Heaton 1983;  
147 Beroza and Spudich 1988), and inversion meth-  
148 ods adopting constrained and simplified kinematic  
149 models (Dreger and Kaverina 2000; Vallée and  
150 Bouchon 2004; Galovic et al. 2009; Cesca et al.

151 2010). All these methods have a significant poten-  
 152 tial for a stable determination of directivity but  
 153 their adoption towards its very fast detection is  
 154 limited, often requiring time consuming computa-  
 155 tion of synthetic seismograms for several extended  
 156 source models. Methods developed by Dreger and  
 157 Kaverina (2000) and following Cesca et al. (2010)  
 158 have shown a good performance and have been  
 159 tested for near real-time applications, but they are  
 160 still based on extended source representations and  
 161 thus require heavier computations with respect to  
 162 our method. Finally, recent results by Zahradnik  
 163 et al. (2008) showed the possibility of discrimi-  
 164 nating the true fault plane on the base of spatial  
 165 offsets between epicentre and centroid locations.  
 166 However, the method has been currently applied  
 167 only to a limited number of earthquakes, with  
 168 variable results, and the determination of directiv-  
 169 ity may be beyond its possibilities, for example for  
 170 symmetric bilateral ruptures.

171 We present here a simple alternative method to  
 172 quickly detect directivity for shallow earthquakes  
 173 and discuss it with the aid of a set of applica-  
 174 tions, including both synthetic datasets and obser-  
 175 vations from recent earthquakes in Greece. Our  
 176 method is based on a point source representation,  
 177 which drastically reduces computational require-  
 178 ments and makes it feasible for early detection.  
 179 Directivity is detected on the basis of a frequency  
 180 domain inversion of the apparent duration at  
 181 each station and the further interpretation of its  
 182 azimuthal variation. Main strength points of the  
 183 proposed method include the adoption of a com-  
 184 mon dataset and modelling tools for focal mech-  
 185 anism and directivity determination, the inclusion  
 186 of Green's functions accounting for wave propa-  
 187 gation through the chosen earth models without  
 188 needing specific aftershocks, and the simplicity  
 189 and quickness of the inversion process.

## 190 2 Directivity and amplitude spectra inversion

191 We make here use of the recently developed  
 192 Kiwi tools (Heimann 2010; Cesca et al. 2010;  
 193 <http://kinherd.org>), which provide a flexible in-  
 194 strument to generate synthetic seismograms for  
 195 point and extended sources and to invert different  
 196 earthquake source parameters, allowing the se-

lection of different waveform tapers, frequency 197  
 filters, inversion domains and misfit functions. 198  
 Cesca et al. (2010) showed successful applications 199  
 to shallow earthquake at regional distances, and 200  
 was able to derive both point source (best double 201  
 couple, DC, model, scalar moment and centroid 202  
 depth) and extended source (fault plane discrim- 203  
 ination, rupture size, rupture time, rupture nucle- 204  
 ation) parameters. 205

The first inversion step follows the approach 206  
 described in Cesca et al. (2010), to obtain the focal 207  
 mechanism, scalar moment and centroid depth: 208

1. Focal mechanism. We invert amplitude spec- 209  
 tra of full waveforms, according to Cesca et al. 210  
 (2010), to derive a point source focal mech- 211  
 anism (DC, depth and scalar moment); the 212  
 source epicentral location is assumed to be 213  
 originally known. 214
2. Polarities. The focal mechanism presents a 215  
 polarity ambiguity, which can be solved by 216  
 comparing observed displacements and syn- 217  
 thetic seismograms for the two possible polar- 218  
 ity configurations; however, the detection of 219  
 the true polarity is here not strictly required, 220  
 as the whole inversion process is carried out 221  
 in the frequency domain, and only amplitude 222  
 spectra are involved in the fitting procedure. 223

The source representation through the Kiwi tools 224  
 allows the adoption of different rise times. For a 225  
 spatially extended source model, where the rup- 226  
 ture region is discretised into a number of spatial 227  
 point sources, the rise time represent the time 228  
 during which each point source radiates seismic 229  
 energy. The duration of the whole rupture process 230  
 is related to rise and rupture times. If we adopt 231  
 a point source representation, the rise time will 232  
 represent the duration of the source time function. 233  
 This parameter was used in Cesca et al. (2010) 234  
 to have a first, rough, estimate of rupture times 235  
 and to choose a proper rise time during kinematic 236  
 source modelling. We proceed here differently: in- 237  
 stead of determining true duration of the rupture 238  
 process, we investigate apparent durations as seen 239  
 by individual stations. 240

In detail, during the second inversion step, we 241  
 proceed as follows (Fig. 1 illustrates an example 242  
 of the main steps, relative to selected seismic 243

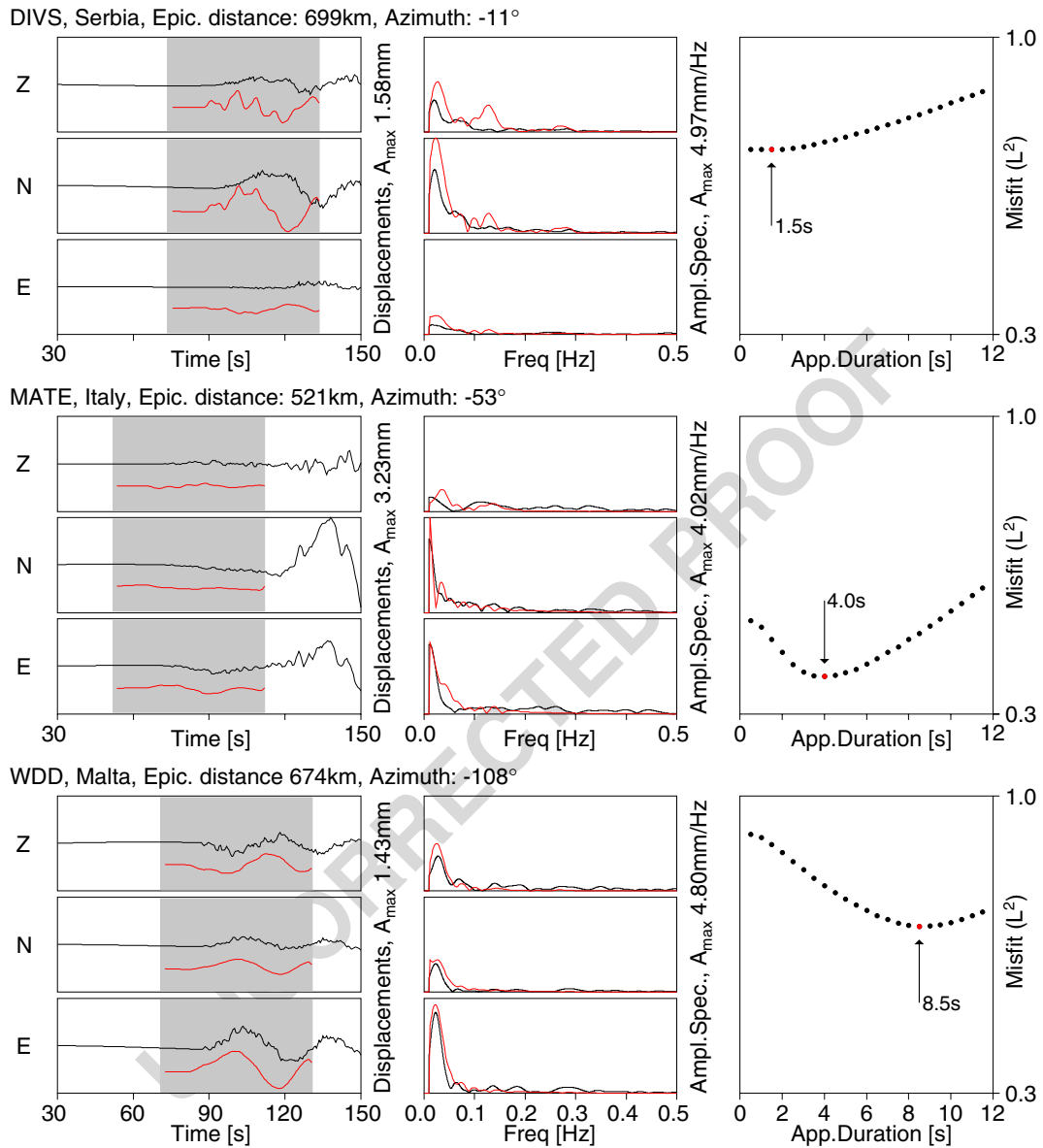


**Fig. 1** Example of the procedure followed to derive the apparent source duration at different stations. Selected waveforms, spectra and amplitude spectra inversion results refer to an application to the Andravida earthquake, Greece, which is further extensively discussed in this study. *Left*: filtered displacements (*black lines*) and synthetic seismograms (*red lines*) for the chosen point source model are

tapered to select P waves time windows (*grey intervals*). *Centre*: amplitude spectra comparison (*red lines* correspond to the best fitting synthetic spectra, after comparing several source durations). *Right*: comparison of amplitude spectra misfit values for different source durations (best solutions for each station are identified by *red circles*)

244 waveforms from the Andravida earthquake,  
245 which is later discussed in the text):

246 1. Waveform selection. We use all available spatial  
247 components, preferably using North, East

and vertical orientations, rather than rotated 248  
traces, in order to have P wave energy on all 249  
traces (which is theoretically null on transversal 250  
components); the presence of more traces 251  
for each station has a smoothing effect; after 252

253 testing with different datasets, we found that  
 254 more components provide more stability. We  
 255 perform a deconvolution of the instrumental  
 256 response from the data, and conversion to  
 257 displacements.

258 2. Tapering. We limit the inversion process to P-  
 259 wave time windows, which are automatically  
 260 selected on the base of the source-receiver  
 261 geometry and theoretical arrival time for the  
 262 earth model used during the inversion (an ar-  
 263 rival time database is calculated in advance, to  
 264 reduce computational effort at the time of the  
 265 inversion); for the case studies here described  
 266 we use 60 s length time windows, starting 15 s  
 267 before theoretical first P arrival, and apply  
 268 a bandpass filter in the range 0.01–0.5 Hz  
 269 (these parameters may be modified depending  
 270 on the earthquake size, the source depth, the  
 271 average duration, and the range of epicen-  
 272 tral distances where waveforms are inverted).  
 273 Tapers should be chosen in order to resolve  
 274 directivity effects. A minimum length should  
 275 account at least for two times the average rup-  
 276 ture duration and for different periods at the  
 277 frequency range used for the inversion. For  
 278 stations located at small epicentral distances,  
 279 with minor delay between S and P phases,  
 280 tapers may be modified to avoid S waves.

281 3. Scalar moment inversion. Since the estima-  
 282 tion of the scalar moment may slightly vary  
 283 depending on the inversion approach (e.g.,  
 284 full waveform or body waves, time domain or  
 285 amplitude spectra inversion, etc.), we mention  
 286 here the possibility to perform a specific in-  
 287 version using an approach consistent with the  
 288 following directivity inversion. Traces from  
 289 all seismic stations would be used to invert  
 290 the scalar moment (e.g. by amplitude spectra  
 291 inversion, using a Levenberg–Marquardt ap-  
 292 proach and an  $L^2$  norm misfit function). In  
 293 the following applications this step is not per-  
 294 formed, as we count with stable estimations of  
 295 the scalar moments, provided by the fit of low  
 296 frequency amplitude spectra from the whole  
 297 waveforms.

298 4. Apparent duration inversion. For each of the  
 299 stations, we perform an amplitude spectra in-  
 300 version to derive the apparent source duration  
 301 at that station; the frequency domain inver-

302 sion approach is less sensitive to unmodelled  
 303 structural heterogeneities; we perform here  
 304 a grid search for possible durations (for the  
 305 following case studies, tested durations varies  
 306 up to 30 s, with an increment of 0.5 s); in  
 307 general we observe smooth single-minimum  
 308 curves of misfit versus apparent durations,  
 309 and tests with different inversion approaches  
 310 (e.g. gradient methods) have shown very con-  
 311 sistent results with respect to the grid walk  
 312 procedure.

The apparent source time function durations can  
 be then quickly interpreted in term of simplified  
 laws for finite rupture models. With the aid of  
 synthetic tests and application to selected earth-  
 quake datasets, we will show that, often, it is not  
 necessary to have a complex rupture model to  
 fit the azimuthal distribution of apparent dura-  
 tions. For simple extended source model, such as  
 a one-dimensional linear source or a Haskell bi-  
 dimensional rupture model (Haskell 1964), the  
 effects of directivity can be treated analytically. A  
 unilateral rupture along a horizontal linear source  
 will produce theoretical P-wave pulses of shorter  
 duration for stations located toward the rupture  
 propagation, and larger duration for stations in  
 the opposite direction. Bilateral ruptures result  
 in a minor azimuthal variation of the apparent  
 source time function. A range of asymmetrically  
 bilateral rupture models exists in between. Effects  
 of oblique and vertical rupture propagations may  
 also be modelled but are more difficult to reveal  
 (Beck et al. 1995) and have been more rarely  
 observed (e.g. Eshghi and Zare 2003; Nadim et al.  
 2004).

We originally focus on the two-dimensional  
 problem, with source and observer laying on the  
 same plane. Let us assume a horizontal linear  
 source model of length  $L$ , with the rupture starting  
 at one edge (A) and propagating unilaterally till  
 the other edge (B). The rupture time  $t_R$  is the time  
 required for the rupture front to propagate along  
 the entire rupture length, from A to B, at a rupture  
 velocity  $v_R$ , which is assumed to be constant. The  
 rise time  $t_r$ , defined as the duration of seismic  
 source emission from a point along the source, is  
 here assumed to be constant, according to healing  
 front theory (Nielsen and Madariaga 2003) and

350 will be further considered negligible with respect  
 351 to the rupture time. Finally,  $v_P$  is the average P  
 352 wave velocity at the focal region. Typically, rup-  
 353 ture propagates with a velocity slightly below the  
 354 shear wave velocity at the focal region, which also  
 355 shows a common scale with compressional wave  
 356 velocity in seismogenic regions. Then, according  
 357 to Ben-Menahem and Singh (1981), and including  
 358 the rise time, for a receiver located at azimuth  $\varphi$   
 359 (defined with respect to the direction of rupture  
 360 propagation) the apparent source duration  $\Delta t(\varphi)$   
 361 will be given by:

$$\Delta t(\varphi) = t_r + \frac{L}{v_R} - \frac{L}{v_P} \cos(\varphi). \tag{1a}$$

362 In view of a more general formulation, also ac-  
 363 counting for asymmetric and pure bilateral rup-  
 364 ture, the rupture length  $L$  is divided into two  
 365 segments  $L_1$  and  $L_2$ , with the following expression  
 366 for the apparent source duration  $\Delta t(\varphi)$ :

$$\Delta t(\varphi) = \text{Max} \left[ t_r + L_1/v_R - (L_1/v_P) \cos(\varphi), \right. \\ \left. t_r + L_2/v_R + (L_2/v_P) \cos(\varphi) \right] \tag{1b}$$

367 We can then introduce the following non-  
 368 dimensional variables:  $\tau(\varphi)$  is the ratio between  
 369 the apparent source duration  $\Delta t(\varphi)$  and the rup-  
 370 ture time  $t_R$ ,  $t_{r/R}$  is the ratio between rise and  
 371 rupture time,  $v_{R/P}$  is the ratio between rupture  
 372 velocity and P wave velocity at the source;  $L_1$  and  
 373  $L_2$  ( $L_1 \geq L_2$ ) are expressed as  $(1-\chi)L$  and  $\chi L$ ,  
 374 respectively,  $\chi$  being the ratio between the short-  
 375 est segment and the entire rupture length ( $\chi$  may  
 376 range from 0, for a pure unilateral rupture, to 0.5,  
 377 for a pure bilateral one). The azimuthal depen-  
 378 dency of  $\tau(\varphi)$ , making use of the non-dimensional  
 379 notation is the following ( $t_{r/R}$  can be in general  
 380 neglected):

$$\tau(\varphi) = \text{Max} \left[ t_{r/R} + 1 - v_{R/P} \cos(\varphi), \right. \\ \left. t_{r/R} + L_2/L_1 + L_2/L_1 \cos(\varphi) \right]. \tag{2}$$

381 The radiation pattern for three significant cases  
 382 (pure unilateral, pure bilateral and asymmetric  
 383 bilateral) is shown in Fig. 2, where we have chosen  
 384  $v_{R/P} = 0.5$  ( $v_{R/P}$  equal to 0.25 and 1.0 for the slow  
 385 and fast cases respectively),  $\chi$  is equal to 0, 1/3  
 386 and 1/2 for the three considered cases. We choose  
 387 different rupture lengths  $L$ , in order to have a  
 388 constant length of the largest rupture segment.

Symmetries of apparent duration radiation pat- 389  
 terns can be observed, with a one lobe shape for 390  
 a pure unilateral rupture and a two lobe shape for 391  
 a pure bilateral one. The theoretical curve of the 392  
 apparent rupture duration (Fig. 2, right) for the 393  
 unilateral case range from  $t_r + t_R - t_P$  (azimuth of 394  
 rupture direction) to  $t_r + t_R + t_P$  (opposite direc- 395  
 tion); its average value is equal to  $t_r + t_R$  (for a 396  
 unilateral rupture model  $t_R$  and  $t_P$  are the rupture 397  
 time and P wave travel time along the entire 398  
 rupture length). For the pure bilateral rupture, the 399  
 apparent duration varies between  $t_r + t_R$  (perpen- 400  
 dicular to rupture direction) to  $t_r + t_R + t_P$  (paral- 401  
 lel to rupture direction), with  $t_R$  and  $t_P$  referring 402  
 here to half of the rupture length. The larger vari- 403  
 ation of the apparent duration for the unilateral 404  
 case, with respect to the bilateral, explains the 405  
 major difficulties in observing directivity for the 406  
 second case. Less known is the behaviour of asym- 407  
 metric bilateral ruptures, although this model is 408  
 the most general. In this case the radiation pat- 409  
 tern (Fig. 2, bottom) present a deformed one- 410  
 lobe shape, with the minimum observed apparent 411  
 rupture duration at about  $45^\circ$  from the rupture di- 412  
 rection of the largest rupture length. The azimuth 413  
 $\alpha$ , where a cusp-like minimum in the apparent 414  
 duration may be observed, can be obtained by 415  
 equalizing the two right terms in Eq. 2: 416

$$\alpha = a \cos \left[ \frac{(1 - 2\chi)}{v_{R/P}} \right]. \tag{3}$$

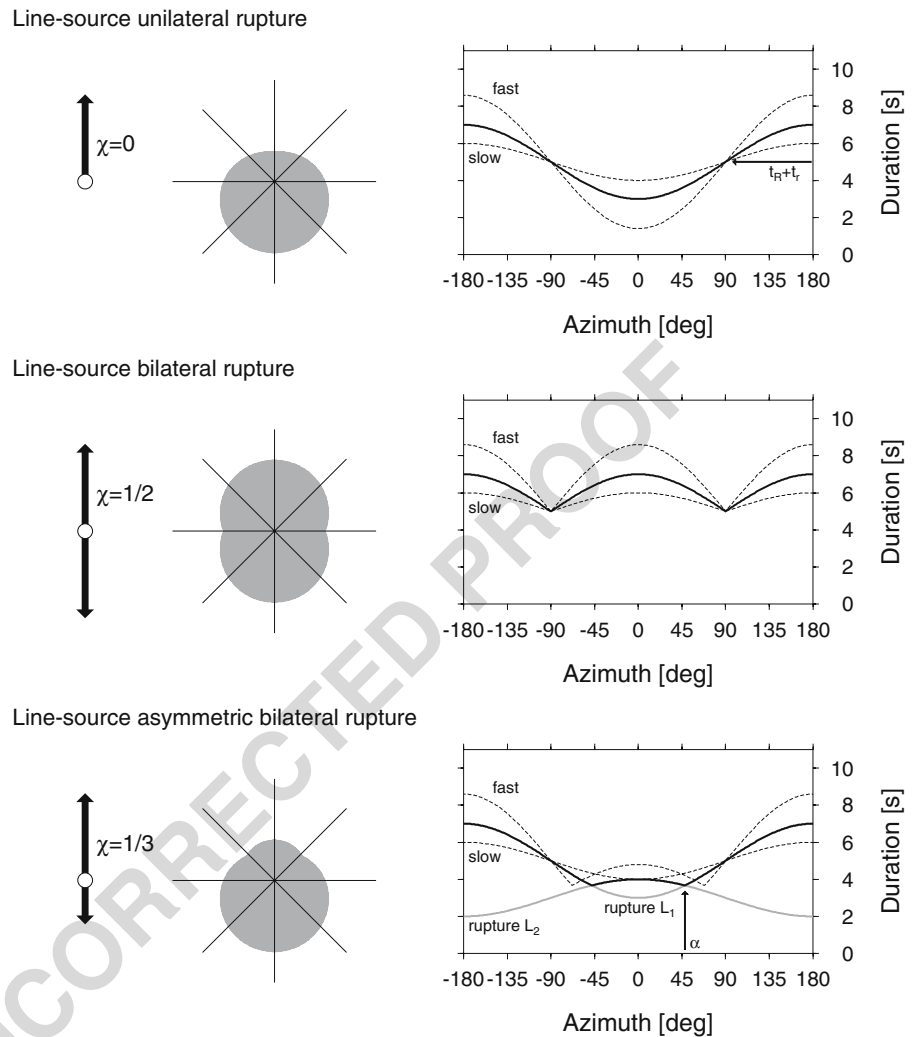
Since  $v_R$  pertains to  $[0, v_P]$ , it follows that for a 417  
 pure unilateral rupture ( $\chi = 0$ ) we have a single 418  
 minimum in direction of rupture propagation, 419  
 while cusp-like minima are not observed. For a 420  
 pure bilateral rupture ( $\chi = 0.5$ ),  $\alpha = \pm\pi/2$  always. 421  
 For the intermediate case of asymmetric bilateral 422  
 ruptures ( $0 < \chi < 0.5$ ), two cusp-like minima are 423  
 observed if the following condition is met: 424

$$\chi > \frac{(1/v_{R/P})}{2}. \tag{4}$$

This means that the observation of two minima in 425  
 the apparent duration curve indicate a dominant 426  
 bilateral rupture processes. 427

Figure 2 additionally shows how larger vari- 428  
 ations in the apparent duration estimations are 429  
 found, when increasing the rupture velocity (in 430  
 the figure, effects for an extreme case of  $v_R =$  431

**Fig. 2** Theoretical models for pure unilateral (*top*), pure bilateral (*centre*) and asymmetric bilateral (*bottom*) line sources. The ruptures start at a nucleation point (*white circles, left plots*) and propagate along segments  $L_1$  and  $L_2$  (*black arrows*), producing different apparent duration radiation patterns (*grey regions, central plots*) which have an azimuthal dependence. *Right plots* present the curves of the apparent duration versus azimuth: *thick black lines* represent an average behaviour ( $v_R = 0.5v_P$ ), while *dashed lines* represent fast ( $v_R = v_P$ ) and slow ( $v_R = 0.25v_P$ ) rupture cases. In the case of a partial unilateral rupture, the curve of apparent duration for the average case (*thick black line*) is given by the maximum of the curves associated to unilateral ruptures along the two segments (*thick grey lines*)



432  $v_P$  are considered). On the other hand, a slower  
 433 rupture tends to behave similarly to a spatial point  
 434 source model (with a finite time duration); Fig. 2  
 435 shows the case of  $v_R = 0.25v_P$ , a proportion which  
 436 is not unrealistic and can be proper for shallow  
 437 earthquake in sediment layers (e.g. Selby et al.  
 438 2005; Dahm et al. 2007).

439 For a 3D earth model, directivity effects do not  
 440 depend only on station azimuth but also on take-  
 441 off angles. Equations 1a, 1b and 2 will then depend  
 442 on the angle between the rupture direction and  
 443 the ray direction at the source, instead than on sta-  
 444 tion azimuth. These considerations opened space  
 445 for specific detailed inversion approaches, such  
 446 as the successful study by Warren and Shearer  
 447 (2006), which accounted for take off angles and

required a dense station distribution both in terms 448  
 of azimuthal coverage and range of epicentral dis- 449  
 tances. We discuss here the problem for the case 450  
 of unilateral rupture. A first observation is that 451  
 even for the same source-receiver configuration, 452  
 different rays travelling along different paths, with 453  
 different take-off angles, will present different 454  
 directivity effects. For any considered bodywave 455  
 with take-off angle  $\theta$ , we predict theoretically a 456  
 minor variability of the apparent duration with 457  
 respect to the one modelled for a planar case. For 458  
 example, the maximal apparent duration, at the 459  
 azimuth opposite to the direction of the rupture 460  
 propagation, will be equal to  $t_r + t_R + t_P \cos(\theta)$ , 461  
 which differs from Eq. 1a. Additionally, we have 462  
 the superposition of different P wave arrivals, with 463



464 different take-off angles. In any case, the interpre-  
 465 tation of the maximal apparent duration following  
 466 Eq. 1a and neglecting take-off angles and rise time  
 467 effects will lead to an overestimation of the terms  
 468  $t_R$  and  $t_P$  and consequently an overestimation of  
 469 the rupture length. The value derived in such ap-  
 470 proximation can be safely considered as an upper  
 471 bound to the real rupture length.

472 Our approach here is to model only the az-  
 473 imuthal variation of directivity effects. The ap-  
 474 proximation is limited by different conditions.  
 475 First, we will focus on shallow earthquakes and  
 476 use only regional distances seismograms (epicen-  
 477 tral distances in the range 200–1,000 km), basing  
 478 our inversion on the fit of time windows centred at  
 479 the first P wave arrivals. Additionally, we will con-  
 480 sider only the case of horizontal to sub-horizontal  
 481 ruptures (rupture propagating along direction dip-  
 482 ping at most  $20^\circ$ ). In these circumstances, we will  
 483 show that the main rupture propagation can be  
 484 detected even with the approximated approach  
 485 here described. The interpretation of additional  
 486 rupture parameters is strongly limited by neglect-  
 487 ing take-off angles and rise time effects, and the  
 488 derived rupture length should be considered as an  
 489 upper bound to its real value.

490 On the base of the previous discussion, we can  
 491 now explain the last step of the inversion ap-  
 492 proach, where the distribution of apparent source  
 493 time durations is interpreted in terms of simplified  
 494 rupture models:

- 495 1. Point source model. If we assume a spatial  
 496 point source model, with a given source time  
 497 function of duration  $t_r$ , the curve of appar-  
 498 ent duration will be a straight line, with no  
 499 azimuthal dependence. This is the particular  
 500 case, which can also be described by the pre-  
 501 vious equations, with  $L = 0$ , which leads to  
 502  $t_R = t_P = 0$ . The model has a unique unknown,  
 503  $t_r$  (by definition, rise time), which represents  
 504 the apparent rupture time everywhere.
- 505 2. Pure/predominant unilateral rupture. In this  
 506 case, the azimuthal distribution of apparent  
 507 durations is expected to follow a sinusoidal be-  
 508 haviour. The fit is expected to be larger in case  
 509 of a pure unilateral rupture, but the model can  
 510 still well reproduce data also for asymmetric  
 511 bilateral ruptures. In both cases, the minimum

of the curve will indicate the main rupture 512  
 direction ( $\varphi_0$ ). The model is represented by 513  
 the curve of the apparent duration  $\Delta t(\varphi)$ : 514

$$\Delta t(\varphi) = -A \cos(\varphi - \varphi_0) + B \quad (5)$$

with A and B positive, describing in first approx- 515  
 imation the travel time of P waves along the rup- 516  
 ture length ( $t_P$ ) and the sum of rise and rupture 517  
 times ( $t_r + t_R$ ). 518

3. Pure bilateral rupture. In case of a pure bilat- 519  
 eral rupture, we will use the following curve, 520  
 instead: 521

$$\Delta t(\varphi) = A |\cos(\varphi - \varphi_0)| + B. \quad (6)$$

4. Comparison of directivity models. Since 522  
 Eqs. 5 and 6 are dependent on three unknown 523  
 parameters, while the standard average rup- 524  
 ture time has only one (the average earth- 525  
 quake duration or duration of the common 526  
 source time function), they will always pro- 527  
 vide a better fit with respect to the common 528  
 rupture duration model. An  $F$  test can than 529  
 be used to evaluate the misfit improvement 530  
 versus the increase of degrees of freedom.  $F$  531  
 values above 0.5 will be used here to prefer 532  
 unilateral or bilateral models with respect to 533  
 the point source solution. The modelling of 534  
 asymmetric bilateral rupture requires more 535  
 free parameters, being the superposition of 536  
 two functions as in Eq. 5. Chances for the im- 537  
 plementation of such a model are highly lim- 538  
 ited by several factors, including data quality, 539  
 focal mechanism, epicentral azimuthal cover- 540  
 age and local structural heterogeneities. We 541  
 suggest here the adoption of this model only 542  
 for specific cases rather than its implementa- 543  
 tion within the automated processing. 544

The major advantages of the presented approach 545  
 are that only point source synthetic seismograms 546  
 are used, so that forward modelling and inversion 547  
 are fast. A second advantage lies in the intrinsic 548  
 simplicity of this approach, which provides simple 549  
 plots of easy interpretation and suggest its imple- 550  
 mentation for automated routines. In the worse 551  
 case, if no clear pattern is detected, the retrieved 552  
 information can still be used to better focus a 553  
 more detailed full waveform kinematic inversion 554

(e.g., as in Cesca et al. 2010), by limiting the range of rupture times and/or spatial extension to be tested. A last important advantage resides in the coherency of the inversion approach: we use the same tools and the same data to derive first the focal mechanism (or moment tensor) and to detect directivity effects, instead of relying on an externally calculated focal mechanism solution, which may be biased by a specific selection of stations, earth model, and processing routines. An important limitation of the method applicability is represented by a specific range of earthquake magnitudes. For small earthquakes, with the rupture process occurring in less than 2 s, the variation of the apparent rupture duration could be only detected by fitting high frequency spectra (up to 0.5 Hz or above), which requires a detailed knowledge of the crustal structure, and possibly the adoption of 3D earth models. On the opposite side, large earthquakes may present more complex rupture processes, with different slip patches or asperities, breaking at different times. Large earthquakes also present significant discrepancies between hypocentral and centroid locations. Both effects are not considered in our model and can then lead to erroneous interpretations. As a rule of thumb, we believe that earthquakes with magnitudes in a range  $M_w$  5.5–7.0 may be the best suited for a successful application.

### 3 Synthetic tests for linear and planar sources

Before applying the method to real data, and in order to assess the method performance, we carry out a set of inversions using synthetic datasets. We generate synthetic seismograms first for linear sources and consequently to planar ones. Considered source models present different significant focal mechanisms and directions of rupture propagation. Both synthetics for linear and planar sources are generated using the Kiwi tools (<http://kinherd.org>; Heimann 2010), assuming the PREM model (Dziewonski and Anderson 1981). The inversion is then carried out as described in the previous paragraph, assuming a spatial point source. Focal mechanisms, scalar moment and depth are retrieved at a first stage, by using the method described in Cesca et al. (2010), which has

been here specifically modified in order to include the retrieval of the apparent rupture time at each station. In the synthetic tests, a dense grid of 154 stations is considered, in order to plot apparent duration contours. Stations location accomplish to the chosen conditions in terms of epicentral distances.

Three line source mechanisms (strike-slip (SS) strike  $\varphi = 30$ , dip  $\delta = 90$ , rake  $\lambda = 0$ ; normal fault (NF)  $\varphi = 30$ ,  $\delta = 45$ ,  $\lambda = 90$ ; thrust fault (TF)  $\varphi = 30$ ,  $\delta = 20$ ,  $\lambda = -90$ ) and three rupturing models (pure unilateral, asymmetric bilateral, pure bilateral) are considered at first, thus providing a set of nine source models. Ruptures propagate horizontally for the strike-slip and normal fault, in direction NNE–SSW, and toward ESE along the low-angle dipping plane, for the thrust fault. The source model centroid is always located at a depth of 20 km, the source length is 30 km, rupture velocity is 3.5 km/s. Pure unilateral ruptures start at the southern (SS, NF) or western (TF) edge. The same main rupture direction is used for asymmetric bilateral ruptures, the two ruptured segments having lengths  $L_1 = 22.5$  and  $L_2 = 7.5$  km. Rise time is fixed to 2 s in all cases. The inversion is carried out using 40 s time windows, starting 10 s before the theoretical arrival of P phases. A frequency bandpass, between 0.01 and 0.5 Hz, is used to filter Green's functions and data. Inversion results are shown in Fig. 3. Coloured surface, representing the inverted apparent source duration, highlight the radiation patterns of apparent duration. The azimuthal distribution of apparent duration clearly shows directivity effect and its minor dependence on epicentral distance using our approach and proof that a good quality fit can be achieved using the simplified azimuthal dependent curves. In particular, the fit of the cosine curve described by Eq. 5 can be used to detect unilateral or asymmetric bilateral ruptures, while the curve from Eq. 6 to detect pure bilateral ruptures. Rupture directivity is correctly detected in all cases, with the exception of the bilateral rupture along the low-dipping angle plane of the thrust mechanism (Fig. 3, bottom right), where unilateral rupture is incorrectly estimated. The reason for this discrepancy can be described as follows. Since the extended source is not horizontal, the segment toward ESE and WNW are located below

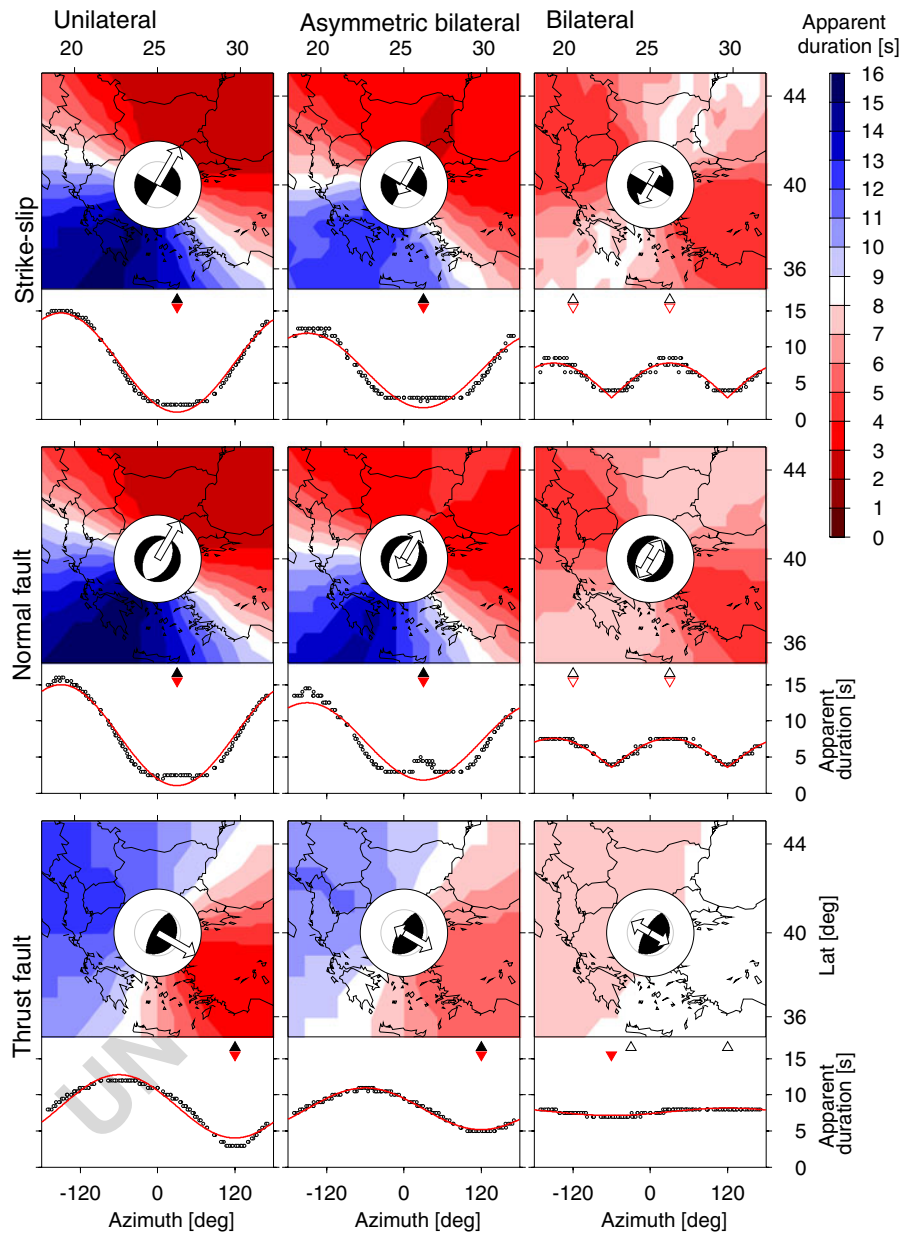


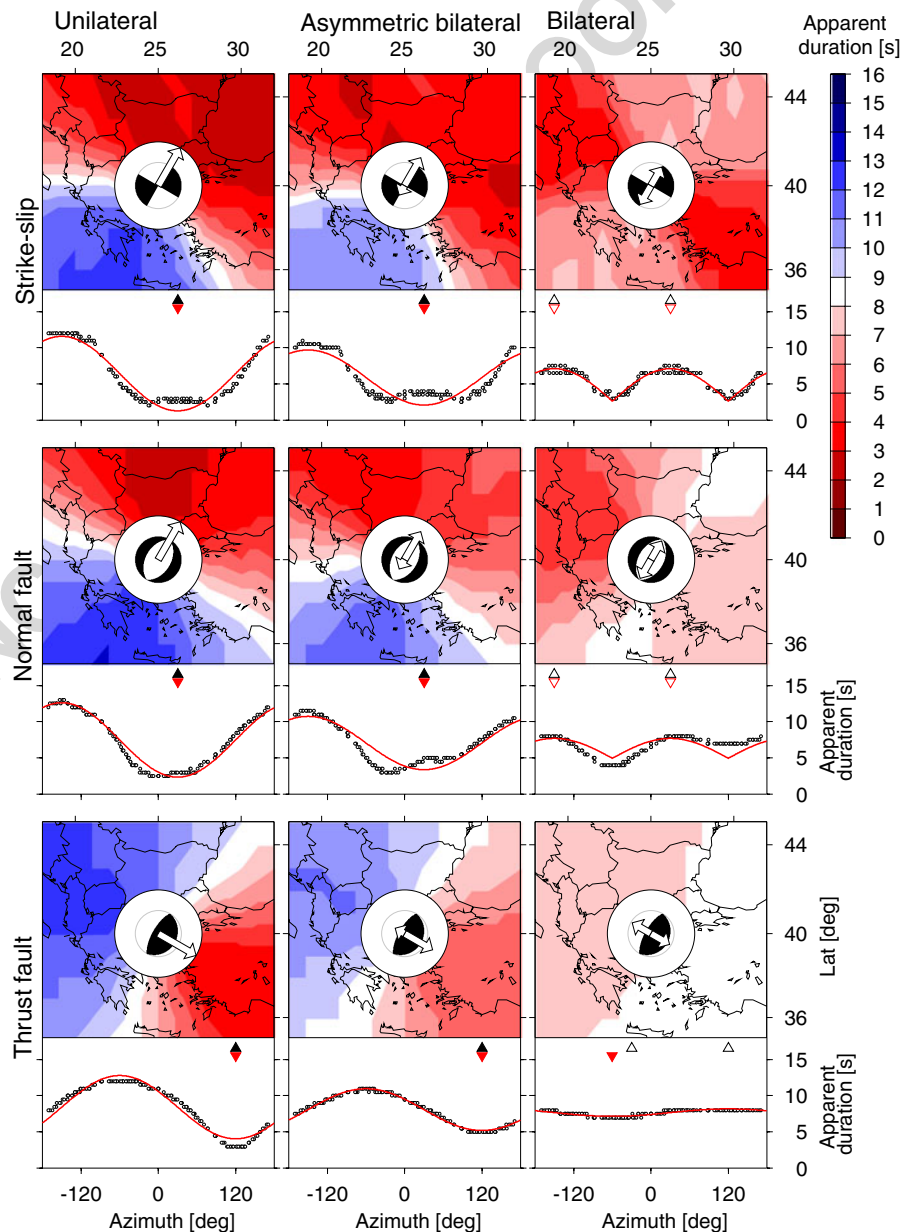
**Fig. 3** Inversion results for linear sources. We consider three focal mechanisms (strike-slip, *top*; normal fault, *centre*; thrust fault, *bottom*) and three rupture processes (pure unilateral, *left*; asymmetric bilateral, *centre*; pure bilateral, *right*). For each case, we show colour plots representing the inverted apparent duration at a dense grid of station around the epicentre (*red to blue scale* represents increasingly longer apparent durations). The focal mechanisms are shown at the epicentral location, together with *white arrows* describing rupture directions (*arrow*

*sizes* are proportional to rupture lengths). *Graphics below each colour plot* represent the apparent duration versus azimuth (*dots*) and the best fitting model (*red curves*). *Upper triangles* represent the correct solution (*a single black triangle* is plotted at the proper azimuth for unilateral and asymmetric bilateral ruptures; *two white triangles* indicate rupture directions for pure bilateral rupture cases). *Inverted triangles* represent inversion results (*single red triangle* for unilateral and asymmetric bilateral ruptures, *two white triangles* for pure bilateral ruptures)

650 and above the centroid depth, respectively. Since  
 651 we use a layered model, the frequency content  
 652 of synthetic seismogram varies from shallower to  
 653 deeper sources, as well as take off angles. These  
 654 effects, which cannot be reproduced by a point  
 655 source located at the centroid depth, results larger  
 656 than those related to the bilateral rupture, thus  
 657 explaining the detection of an apparent directivity  
 658 towards dip direction.

Given the successful application to line sources, 659  
 we simulate now more realistic rupture processes, 660  
 generating synthetic seismograms for the eikonal 661  
 source model (Heimann 2010; Cesca et al. 2010). 662  
 We use here circular faults, with rupture propagat- 663  
 ing with a variable velocity, scaling by a coefficient 664  
 0.9 with shear wave velocity in the crustal model. 665  
 Given the adoption of the PREM model, the 666  
 source depth and its extension, rupture velocity 667

**Fig. 4** Inversion results for circular eikonal sources. For each of the nine considered source models, we show colour plots representing the inverted apparent duration around the epicentre (*red to blue scale* represents increasingly longer apparent durations). Graphics below each coloured plot represent the apparent duration versus azimuth (*dots*) and the best fitting model (*red curves*). We use the same symbol convention as in Fig. 3



668 range between 2.9 and 4.0 km/s. Inversion is carried out using the same approach and parameters as for the previous test and results summarized in Fig. 4. The main characteristics of the azimuthal patterns of the apparent rupture duration are preserved. Directivity effects can be detected and modelled for all pure unilateral and asymmetric bilateral ruptures, although the fit quality results in some cases significantly poorer than for line source cases. The adoption of bi-dimensional ruptures, and specifically the inclusion of sources at different depths, slightly modifies the apparent duration pattern, as can be seen by the comparison of plots in Figs. 3 and 4 relative to normal fault mechanism. The modification of the apparent rupture radiation pattern has similar causes than those described for linear sources. Additionally, it is here also depending on the variable rupture velocity (which, according to the crustal model, is faster for deeper sources than for shallower ones). These effects result critical for the inversion of a bilateral rupture for the case of a thrust fault mechanism, which is erroneously interpreted as unilateral (with a rupture propagation in dip direction). On the other hand, the discrimination between pure and asymmetric bilateral rupture is not always possible; the observation of the characteristic lobe associated to the asymmetric bilateral rupture may indicate such a rupture process, but could not be sufficient, alone, to distinguish this case to a pure unilateral rupture.

699 A variation of the scalar moment will lead to a scaling of synthetic seismograms and modify their amplitude spectra. As a consequence, the inversion of apparent durations may lead to slightly different results. In order to investigate these effects, we have perturbed the scalar moments used for synthetic tests, and analyse inversion results. While the uni- or bilateral mode of the rupture and the main rupture direction are not influenced by a variation of the scalar moment and are always correctly retrieved, the rupture time and the following estimation of rupture lengths suffer slight changes. A perturbation of 10% of the correct scalar moment always led to uncertainties below 5% in terms of rupture time and rupture length. Synthetic tests suggest the implementation of the method here proposed towards a rapid detection of directivity effects. Additionally,

717 these tests point out specific cases, where the inversion approach results more critical, and where a careful discussion of results is suggested. In general, horizontal ruptures and pure or partially unilateral ruptures are more easily detected, whereas pure bilateral sources and rupture propagating along dipping directions may be more problematic to resolve.

#### 4 The Andravida 8.6.2008 earthquake

725 On June 8th, 2008, a magnitude Mw 6.4 earthquake struck NW Peloponnese, Greece. The earthquake, here further referred as the Andravida earthquake, produced two casualties, about 100 injuries and several damages (Chouliaras 2009). A wide number of studies covered the earthquake source and its effects. A pure strike-slip focal mechanisms was unanimously provided by several institutions and catalogues surveying regional and global seismicity, including National Observatory in Athens (NOA), Aristotle University of Thessaloniki (AUTH), INGV European-Mediterranean RCMT Catalogue (INGV-RCMT), Swiss Federal Institute of Technology, United States Geological Survey (USGS) and Global CMT Catalogue (CMT). According to these models, fault planes are almost vertical and oriented NNE–SSW and WNW–ESE. Source depth estimations showed some variability, ranging between 10 and 38 km, and magnitudes Mw ranged between 6.3 and 6.5. The epicentral locations of the earthquake aftershocks (Ganas et al. 2009; Gallovic et al. 2009; Kostantinou et al. 2009), which are distributed within a narrow strip extending NNE–SSW, provide a convincing image of the rupture orientation. The cloud of aftershocks elongates for about 30–35 km, providing a first rough estimation of rupture size. The aftershock distribution is denser towards the Northern edge. To the south, epicentral locations may indicate a minor bending of the rupture area to a slightly larger strike. All published source models are consistent with the identification of the NNE–SSW striking fault plane. Sokos et al. (2008), using hypocentral-centroid relative location method, identified the same plane; since centroids locations are generally

763 located North of hypocentral locations, some indi-  
 764 cation for a dominant propagation towards North  
 765 may arise from this study. Even more convincing,  
 766 with respect to the detection of directivity, are  
 767 the studies of Kostantinou et al. (2009), Gallovic  
 768 et al. (2009) and Cesca et al. (2010). The first  
 769 authors derived a finite source model, also con-  
 770 sistent with their aftershock relocations, finding  
 771 a rupture length of 22.4 km and an asymmetric  
 772 bilateral rupture, with a major rupture along the  
 773 NE branch. Gallovic et al. (2009) used a conjugate  
 774 gradient method to detect the spatio-temporal  
 775 evolution of the rupture process. Results indicate  
 776 a predominantly unilateral rupture, propagating  
 777 along a main slip patch, with a rupture length  
 778 of about 20 km and a rupture velocity of about  
 779 3 km/s. Cesca et al. (2010), based on amplitude  
 780 spectra inversion of full waveform and assuming

an eikonal source model, detected an asymmetric 781  
 rupture propagation, with a predominance of 782  
 rupture propagation towards NNE; the rupture 783  
 length was estimated 40 km, while the average 784  
 rupture velocity was fixed to about 3.2 km/s. The 785  
 consistency of these results (see Fig. 5 bottom), 786  
 obtained with different methods and datasets, 787  
 offer a serious reference to our study in terms of 788  
 fault plane identification and rupture directivity. 789

In our inversion, we assume the epicentral loca- 790  
 tion provided on the EMSC-CSEM webpage 791  
 and the focal mechanism determined by Cesca 792  
 et al. (2010), which is based on the fit of full 793  
 waveform amplitude spectra. We observed that 794  
 a new estimation of the scalar moment, based 795  
 on the fit of P wave spectra only, would present 796  
 minor variation with respect to the assumed value 797  
 (5.97e18 instead of 6.07e18 Nm). Then, we invert 798

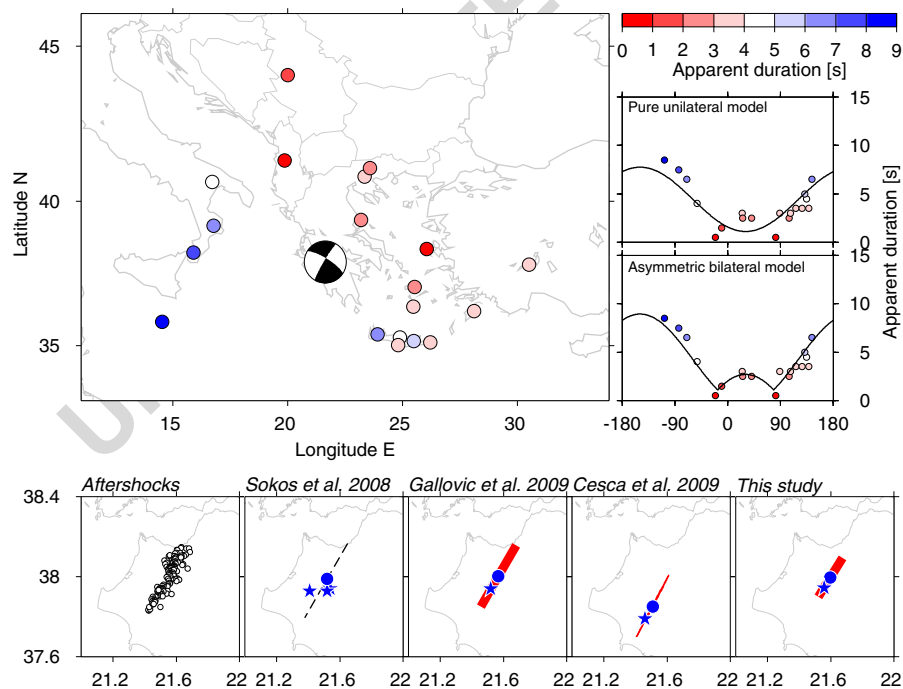


**Fig. 5** Inversion results for the Mw 6.4 Andravida (NW Peloponnese) earthquake (*top*) and comparison with published source models (*bottom*). *Top*: coloured dots represent the inverted apparent duration at the stations used, according to the given colour scale; the azimuthal distribution of apparent durations may be fitted (*top right*) assuming a pure unilateral or, better, a partially unilateral rupture (*thick lines*). *Bottom*: the comparison of aftershocks distribution (after Gallovic et al. 2009) identifies

the NNE–SSW rupture plane in agreement with centroid-hypocentral technique (Sokos et al. 2008), adjoint method (Gallovic et al. 2009), full waveform kinematic inversion (Cesca et al. 2010) and our results; the last four methods consistently detect a partially unilateral rupture towards NNE. Stars and blue circles represent here nucleation points and centroids respectively; the rupture area is plotted in red

799 for the apparent duration at each station sep- 848  
 800 arately and plot resulting values in function of 849  
 801 station azimuth (Fig. 5), according to the discussed 850  
 802 methodology. As a first approximation, we try to 851  
 803 fit apparent durations by means of pure unilateral 852  
 804 and pure bilateral rupture models, assuming both 853  
 805 fault planes. Since fault planes are almost vertical, 854  
 806 only horizontal directions of the rupture velocity 855  
 807 along these planes are considered. The unilateral 856  
 808 rupture model with rupture propagation towards 857  
 809 NNE provide a very good fit to the apparent du- 858  
 810 ration data, and is preferred to remaining models 859  
 811 on the base of the F test. This result provides a 860  
 812 clear indication for a rupture propagating towards 861  
 813 NNE, and thus can be used to discriminate the 862  
 814 true fault plane (NNE–SSW) from the auxiliary  
 815 one (WNW–ESE). Based on the good fit, we try  
 816 to refine our solution by investigating asymmetric  
 817 bilateral ruptures. Results provide an even more  
 818 convincing fit (Fig. 5, bottom right), when an  
 819 asymmetric bilateral source model with rupture  
 820 propagating mostly Northward is assumed, as the  
 821 curve account for the two symmetric minima at  
 822 about  $-21.5$  and  $82.5^\circ$  and the internal charac-  
 823 teristic lobe of asymmetric rupture (see Fig. 2,  
 824 bottom). On the other side, this result is in very  
 825 good agreement with published models discussed  
 826 before. According to the previous discussion for  
 827 a simplified bidimensional case, the maxima of  
 828 the two cosine curves associated to the rupturing  
 829 of two segments of the fault are equal to  $t_P +$   
 830  $t_R + t_r$ , where these terms refer to the P wave  
 831 propagation, rupture and rise time related to each  
 832 segment. The maxima of the apparent duration  
 833 curve are equal to 8.9 s (segment  $L_1$  toward NNE)  
 834 and 2.7 s (segment  $L_2$  toward SSW). Assuming  
 835 an average P wave velocity of 8 km/s (consistent  
 836 with the used velocity model at the hypocentral  
 837 depth), a rupture velocity of 3 km/s (consistent  
 838 with Gallovic et al. 2009), and considering the rise  
 839 time negligible with respect to rupture time, we  
 840 obtain rupture lengths of about 19 and 6 km. The  
 841 total length of about 25 km for the main patch  
 842 is in general agreement with most of published  
 843 results. We observe a discrepancy with the rupture  
 844 size of about 40 km determined in Cesca et al.  
 845 (2010). This last value might be overestimated,  
 846 as the adopted full waveform kinematic inversion  
 847 may in some cases be affected by a trade-off be-

tween different source parameters. The observed 848  
 discrepancy may also indicate a different response 849  
 of the two approaches to the rupture process and 850  
 energy emission, with the full waveform inver- 851  
 sion detecting the largest rupture length, and the 852  
 directivity inversion identifying the main rupture 853  
 patch. The upper limit value we found here is 854  
 slightly larger than the length estimated by stan- 855  
 dard empirical relations (according to Wells and 856  
 Coppersmith 1994, the average rupture length for 857  
 a Mw 6.4 is about 14 km). We remark that the 858  
 interpretation of inversion results to this extent 859  
 should be carried out only in best conditions, 860  
 where the fitting of the apparent duration curve 861  
 is good enough to further interpret it. 862

## 5 The SW Peloponnese 14–20.2.2008 seismic 863 sequence 864

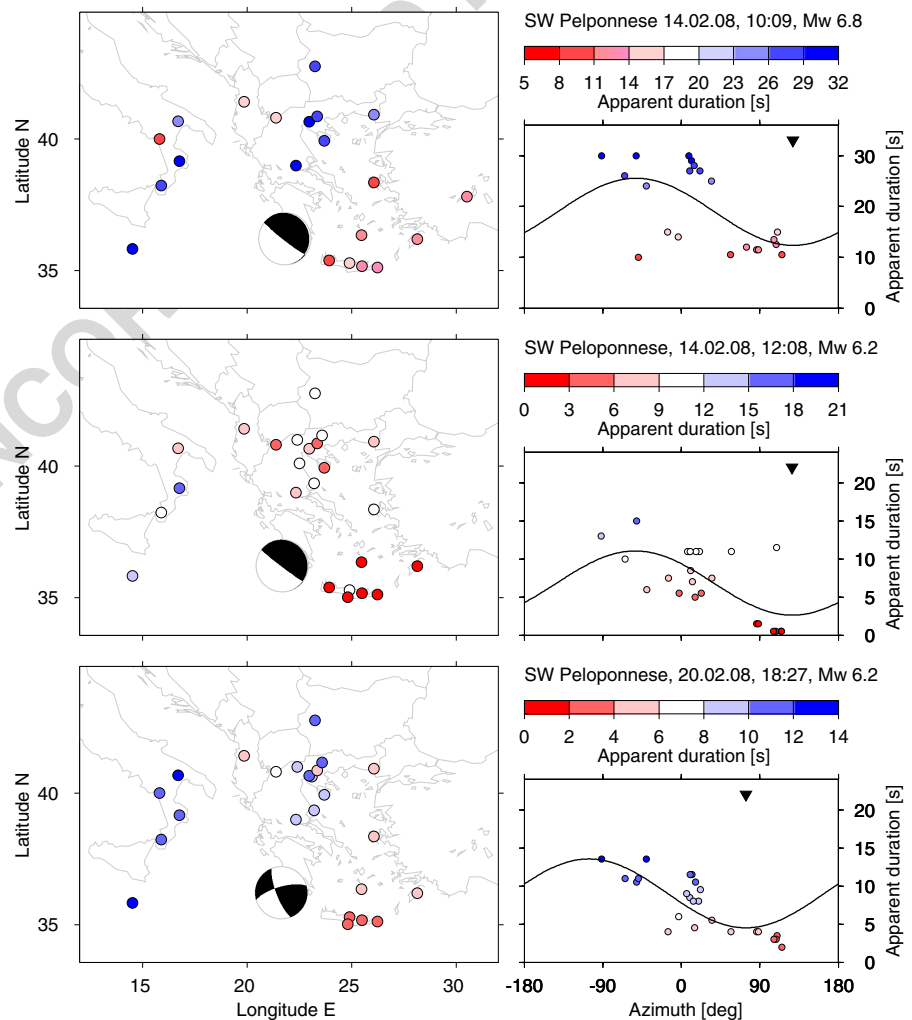
A seismic sequence struck the region offshore 865  
 SW Peloponnese, Greece, in the days following 866  
 February 14th, 2008, with three major earth- 867  
 quakes occurring within a week. On February 868  
 14th, a first Mw 6.8 (magnitude estimated by 869  
 EMSC-CSEM and Cesca et al. 2010) event struck 870  
 the region at 10:09 UTC. Two hours later, at 871  
 12:08, UTC, a Mw 6.2 aftershock occurred. Fi- 872  
 nally, on February 20th (18:27 UTC), a Mw 6.2 873  
 event took place. Focal mechanisms (EMSC- 874  
 CSEM webpage) indicate thrust faulting for the 875  
 first two events, while the last one has a different, 876  
 strike-slip mechanism, with fault planes striking 877  
 ENE and NNW. Source depths, according to 878  
 EMSC-CSEM catalogue, were 30, 20 and 25 km, 879  
 respectively, for the three earthquakes. Whereas 880  
 different institutions (e.g. NOA, AUTH, Uni- 881  
 versity of Patras UPSL, INGV-RCMT, USGS, 882  
 CMT) provided point source solutions for these 883  
 events, few trials has been carried out so far to 884  
 interpret rupture kinematics (Roumelioti et al. 885  
 2009; Cesca et al. 2010). A strongly uneven sta- 886  
 tion distribution and large epicentral gaps toward 887  
 SW have possibly limited source modelling until 888  
 now. Based on full waveform inversion, Cesca 889  
 et al. (2010) identified the ENE–WSW plane for 890  
 the strike-slip earthquake of February 20th, and 891  
 a partial unilateral rupture towards the coast was 892  
 found. For the first two earthquakes, the low angle 893

894 planes dipping toward NW were preferred, but the  
 895 inversion results were not completely satisfacto-  
 896 rily. Roumelioti et al. (2009) adopted an empirical  
 897 Green's functions approach, using the Mw 6.2  
 898 aftershock to model the finite fault of the largest  
 899 earthquake; their results support the identification  
 900 of the low angle dipping plane as well as directivity  
 901 towards SSW. Finally, the identification of low  
 902 dip angle rupture planes in this region for thrust  
 903 earthquakes would agree with local tectonics, as-  
 904 sociating the earthquake occurrence to oceanic  
 905 subduction (Underhill 1999).

906 Figure 6 summarizes our inversion results.  
 907 Differently from the application to the Andravida  
 908 earthquake, apparent durations for the earth-

909 quakes occurring on February 14th show a major  
 910 spreading and are worse fitted by the simplified  
 911 cosine function we associated to pure unilateral  
 912 ruptures. A better fit, and minor spreading, is  
 913 observed for the main event, with respect to its  
 914 aftershock. However, for both two earthquakes, a  
 915 general trend can be detected, indicating a mini-  
 916 mum of the cosine curve for an azimuth of about  
 917 135°, which suggests a main direction of the rup-  
 918 ture propagation towards SE. These results are  
 919 unable by themselves to provide further informa-  
 920 tions about the true fault plane, as they may be  
 921 modelled either assuming the low-angle and the  
 922 steep dipping plane. A better fit is obtained for the  
 923 February 20th earthquake: clear directivity effect

**Fig. 6** Inversion results for the February 14th, 2008, Mw 6.8 (top), the February 14th, 2008, Mw 6.2 (centre) and the February 20th, 2005, Mw 6.2 (bottom) earthquakes, offshore SW Peloponnese. For each earthquake, coloured dots represent the inverted apparent duration at the stations used, according to the colour scale given for each case; the azimuthal distribution of apparent durations (right) may be fitted assuming unilateral ruptures (thick black lines). Inverted triangles indicate the retrieved rupture directions





924 is here retrieved, indicating a rupture mostly prop-  
 925 agating towards ENE, thus along the WSW–ENE  
 926 fault plane. The differentiation between pure or  
 927 partial unilateral rupture may be here rewarded  
 928 as beneath the limit of a safe data interpretation,  
 929 but we observed how the general result is in well  
 930 agreement with previous results by Cesca et al.  
 931 (2010), where the source model was derived by  
 932 the fit of high-frequency (up to 0.1 Hz) amplitude  
 933 spectra from the whole waveforms.

934 Finally, we investigate effects of the assumption  
 935 of imprecise point source parameters on the esti-  
 936 mation of rupture directivity. The effects of anom-  
 937 alous source depth estimation are studied for the  
 938 February 20th aftershock, as different Institutions  
 939 have provided a range of different values ranging  
 940 from 8 to 25 km. We repeated the inversion using  
 941 a different point source solution (strike 249°, dip  
 942 88°, rake −12°, depth 12 km), as provided by the  
 943 INGV European-Mediterranean RCMT Catalog;  
 944 this focal mechanism is similar to our solution and  
 945 major differences concern centroid depth, which is  
 946 now shallower. Directivity inversion remains very  
 947 stable, showing a consistent identification of uni-  
 948 lateral rupture direction toward SE, and indicates  
 949 that a source depth variation of about 10km does  
 950 not result in any significant variation in the radi-  
 951 ation pattern of apparent duration. In a similar way,  
 952 we tested slightly different focal mechanisms for  
 953 both earthquakes of February 14th: even if our fo-  
 954 cal mechanisms are in relatively good agreement  
 955 with other published solutions, some difference  
 956 can be observed. For example, the INGV-RCMT  
 957 catalogue indicates strike angles of 333° and 298°,  
 958 for these earthquakes, which differ from our so-  
 959 lution (347° and 341° respectively). Even in this  
 960 case, after adopting the source parameters pro-  
 961 vided by INGV-RCMT, the inversion results are  
 962 stable, with the detection of main rupture direc-  
 963 tions pointing towards SE–ESE.

## 964 6 Conclusions

965 We propose here a new method for a quick detec-  
 966 tion of directivity effects for shallow earthquakes  
 967 at regional distances. Among the most important

features of the method, we highlight here the 968  
 following ones: 969

- Rapid inversion 970

The assumption of spatial point source allows 971  
 an extremely rapid generation of synthetic seis- 972  
 mograms and point source parameters inversion, 973  
 thus offering a tool to early detect directivity; to 974  
 quantify such improvement, on a standard single 975  
 processor PC the inversion of directivity is here 976  
 carried out within a minute, about 20 times faster 977  
 than the full kinematic inversion for the same 978  
 event, using the approach described in Cesca et al. 979  
 (2010). 980

- Coherent inversion 981

The use of the Kiwi tools for data processing 982  
 and inversions improves significantly the consis- 983  
 tency of our methodology: for example, the same 984  
 dataset and the same inversion tools can be used 985  
 to first derive the focal mechanism, then the scalar 986  
 moment and finally the apparent duration; we 987  
 believe this consistency between data used for 988  
 different inversions significantly improve the co- 989  
 herency of the inversion approach. 990

- Accounting for wave propagation 991

The method is based on amplitude spectra inver- 992  
 sion, using theoretical Green's functions for the 993  
 chosen earth model. In this way, we account for 994  
 wave propagation effect, an improvement with 995  
 respect to standard methods based on pulse length 996  
 estimations. 997

- No requirements of specific aftershocks 998

Avoiding the use of empirical Green's function, 999  
 the method is not limited by the existence of 1000  
 a proper aftershock, nor need to wait for its 1001  
 occurrence. 1002

- Automation 1003

The adoption of the Kiwi tools and the simplicity 1004  
 of the inversion approach made possible the im- 1005  
 plementation of the method as automated routine. 1006

In this manuscript we have demonstrated the 1007  
 method performance, both with a range of syn- 1008  
 thetic tests and with observed data for different 1009

1010 shallow earthquakes recently occurred. These ap-  
 1011 plications offer indications about the quality and  
 1012 extent of inversion results. The retrieval of pure  
 1013 unilateral and pure bilateral ruptures is in gen-  
 1014 eral better resolved than asymmetric ruptures,  
 1015 although the application to the June 8th, 2008,  
 1016 Andravida earthquake showed that this case can  
 1017 also be detected, in favourable conditions. In  
 1018 general, directivity effects are better resolved for  
 1019 strike slip earthquakes, with respect to normal or  
 1020 thrust faulting. Directivity detection offers often a  
 1021 chance to identify the rupture plane, discriminat-  
 1022 ing it from the auxiliary one. The determination  
 1023 of rupture time, rise time and rupture velocity on  
 1024 the base of the proposed method is beyond its  
 1025 purposes and should require a careful supervision.  
 1026 We have here focused to earthquake with magni-  
 1027 tudes of Mw 6 to 7 and shallow hypocentres. The  
 1028 extension of this inversion approach for the study  
 1029 of other range of magnitudes or deeper sources  
 1030 may be investigated in future.

1031 **Acknowledgements** We thank Prof. J. Zahradnik and  
 1032 two anonymous reviewers for useful comments and sug-  
 1033 gestions. The facilities of GEOFON and IRIS Data  
 1034 Management System, and specifically the IRIS Data Man-  
 1035 agement Center, were used for access part of the waveform  
 1036 and metadata required in this study. We acknowledge all  
 1037 institutions providing seismic data used in this research:  
 1038 GEOFON, MEDNET Project, Greek National Seismic  
 1039 Network and Aristotle University Thessaloniki Network.  
 1040 Maps and focal mechanisms have been plotted with GMT  
 1041 (Wessel and Smith 1998). This work has been funded by the  
 1042 German DFG project KINHERD (DA478/14–1/2) and the  
 1043 German BMBF/DFG “Geotechnologien” project RAPID  
 1044 (BMBF07/343).

## 1045 References

1046 Beck SL, Silver P, Wallace TC, James D (1995) Directivity  
 1047 analysis of the deep Bolivian earthquake of June 9,  
 1048 1994. *Geophys Res Lett* 22:2257–2260  
 1049 Ben-Menahem A (1961) Radiation of seismic surface  
 1050 waves from finite moving sources. *Bull Seismol Soc*  
 1051 *Am* 51:401–453  
 1052 Ben-Menahem A, Singh SJ (1981) *Seismic waves and*  
 1053 *sources*. Springer, New York  
 1054 Bernard P, Madariaga R (1984) A new asymptotic method  
 1055 for the modelling of near-field accelerograms. *Bull*  
 1056 *Seismol Soc Am* 74:539–557

Beroza GC, Spudich P (1988) Linearized inversion for fault  
 1057 rupture behaviour: application to the 1984 Morgan  
 1058 Hill, California, earthquake. *J Geophys Res* 93:6275–  
 1059 6296  
 1060 Boore D, Joyner W (1978) The influence of rupture inco-  
 1061 herence on seismic directivity. *Bull Seismol Soc Am*  
 1062 68:283–300  
 1063 Brüstle W, Müller G (1987) Stopping phases in seismo-  
 1064 grams and the spatiotemporal extent of earthquakes.  
 1065 *Bull Seismol Soc Am* 1:47–68  
 1066 Caldeira B, Bezzeghoud M, Borges JF (2009) DIRDOP:  
 1067 a directivity approach to determining the seismic rup-  
 1068 ture velocity vector. *J Seismol* 14:565–600. doi:10.1007/  
 1069 s10950-009-9183-x  
 1070 Cassidy JF (1995) Rupture directivity and slip distribu-  
 1071 tion for the Ms 6.8 earthquake of 6 April 1992,  
 1072 Offshore British Columbia: an application of the em-  
 1073 pirical Green’s function method using surface waves.  
 1074 *Bull Seismol Soc Am* 85:736–746  
 1075 Cesca S, Heimann S, Stammer K, Dahm T (2010) Auto-  
 1076 mated procedure for point and kinematic source inver-  
 1077 sion at regional distances. *J Geophys Res* 115:B06304.  
 1078 doi:10.1029/2009JB006450  
 1079 Chouliaras G (2009) Seismicity anomalies prior to 8 June  
 1080 2008, Mw 6.4 earthquake in Western Greece. *Nat*  
 1081 *Hazards Earth Syst Sci* 9:327–335  
 1082 Dahm T, Krüger F (1999) Higher-degree moment ten-  
 1083 sor inversion using far-field broad-band recordings:  
 1084 theory and evaluation of the method with application  
 1085 to the 1994 Bolivia deep earthquake. *Geophys J Int*  
 1086 137:35–50  
 1087 Dahm T, Krüger F, Stammer K, Klinge K, Kind R,  
 1088 Wylegalla K, Grasso JR (2007) The 2004 Mw 4.4  
 1089 Rotenburg, Northern Germany, Earthquake and its  
 1090 possible relationship with Gas Recovery. *Bull Seismol*  
 1091 *Soc Am* 97:691–704  
 1092 Dreger D, Kaverina A (2000) Seismic remote sensing  
 1093 for the earthquake source process and near-source  
 1094 strong shaking: a case study of the October 16, 1999  
 1095 Hector mine earthquake. *Geophys Res Lett* 27:1941–  
 1096 1944  
 1097 Dziewonski AM, Anderson DL (1981) Preliminary refer-  
 1098 ence earth model. *Phys Earth Planet Int* 25:297–356  
 1099 Eshghi S, Zare M (2003) Reconnaissance report on 26  
 1100 December 2003 Bam earthquake. International Insti-  
 1101 tute of Earthquake Engineering (IIEES)  
 1102 Gallovic F, Zahradnik J, Krizova D, Plicka V, Sokos  
 1103 E, Serpetsidaki A, Tselentis GA (2009) From earth-  
 1104 quake centroid to spatial-temporal rupture evolution:  
 1105 Mw 6.3 Movri Mountain earthquake, June 8, 2008,  
 1106 Greece. *Geophys Res Lett* 36:L21310. doi:10.1029/  
 1107 2009GL040283  
 1108 Ganas A, Serpelloni E, Drakatos G, Kolligri M, Adamis I,  
 1109 Tsimi C, Batsi E (2009) The Mw 6.4 SW-Achaia (west-  
 1110 ern Greece) earthquake of 8 June 2008: seismological,  
 1111 field, GPS, observations and stress modeling. *J Earthq*  
 1112 *Eng* 8:1101–1124  
 1113 Hartzell SH (1978) Earthquake aftershocks as Green’s  
 1114 functions. *Geophys Res Lett* 5:1–4  
 1115

- 1116 Hartzell S, Heaton DV (1983) Inversion of strong ground  
1117 motion and teleseismic waveform data for the fault  
1118 rupture history of the 1979 Imperial Valley, California,  
1119 earthquake. *Bull Seismol Soc Am* 83:1553–1583
- 1120 Hartzell S, Helmberger DV (1982) Strong-motion mod-  
1121 elling of the Imperial Valley earthquake of 1979. *Bull*  
1122 *Seismol Soc Am* 72:571–596
- 1123 Haskell NA (1964) Total energy and energy spectral den-  
1124 sity of elastic wave radiation from propagating faults.  
1125 *Bull Seismol Soc Am* 54:1811–1841
- 1126 Heimann S (2010) A robust method to estimate kinematic  
1127 earthquake source parameters. PhD Thesis, Univer-  
1128 sity of Hamburg, Germany, pp 145
- 1129 Imanishi K, Takeo M (1998) Estimates of fault dimensions  
1130 for small earthquakes using stopping phases. *Geophys*  
1131 *Res Lett* 25:2897–2900
- 1132 Imanishi K, Takeo M (2002) An inversion method to  
1133 analyze rupture process of small earthquakes using  
1134 stopping phases. *J Geophys Res* 107:ESE2.1–ESE2.16.  
1135 doi:10.1029/2001JB000201
- 1136 Kostantinou KI, Melis NS, Lee SJ, Evangelidis CP,  
1137 Boukouras K (2009) Rupture process and aftershock  
1138 relocation of the 8 June 2008 Mw 6.4 earthquake  
1139 in Northwest Peloponnese, Western Greece. *Bull*  
1140 *Seismol Soc Am* 99:3374–3389
- 1141 Li Y, Toksöz MN (1993) Study of the source process of  
1142 the 1992 Columbia Ms = 7.3 earthquake with the em-  
1143 pirical Green's function method. *Geophys Res Lett*  
1144 20:1087–1090
- 1145 Madariaga R (1977) High-frequency radiation from crack  
1146 (stress drop) models of earthquake faulting. *Geophys*  
1147 *J R Astron Soc* 51:625–651
- 1148 Madariaga R (1983) High-frequency radiation from dy-  
1149 namic earthquake fault models. *Ann Geophys* 1:17–23
- 1150 McGuire JJ, Zhao L, Jordan TH (2001) Teleseismic in-  
1151 version for the second-degree moments of earthquake  
1152 space-time distributions. *Geophys J Int* 145:661–  
1153 678
- 1154 McGuire JJ, Zhao L, Jordan TH (2002) Predominance of  
1155 unilateral rupture for a global catalog of large earth-  
1156 quakes. *Bull Seismol Soc Am* 92:3309–3317
- 1157 Müller CS (1985) Source pulse enhancement by deconvolu-  
1158 tion of empirical Green's functions. *Geophys Res Lett*  
1159 12:33–36
- 1160 Nadim F, Moghtaderi-Zadeh M, Lindholm C, Andresen  
1161 A, Remseth S, Bolourchi MJ, Mokhtari M, Tvedt T  
1162 (2004) The Bam earthquake of 26 December 2003.  
1163 *Bull Earthquake Eng* 2:119–153
- 1164 Nielsen S, Madariaga R (2003) On the self-healing fracture  
1165 mode. *Bull Seismol Soc Am* 93:2375–2388
- 1166 Olson AJ, Apsel RJ (1982) Finite faults and inverse theory  
1167 with applications to the 1979 Imperial Valley earth-  
1168 quake. *Bull Seismol Soc Am* 72:1969–2001
- Pro C, Buforn E, Udías A (2007) Rupture length and 1169  
velocity for earthquakes in the Mid-Atlantic Ridge 1170  
from directivity effects in body and surface waves. 1171  
*Tectonophysics* 433:65–79 1172
- Roumelioti Z, Benetatos C, Kiratzi A (2009) the 14 1173  
February 2008 earthquake (M6.7) sequence offshore 1174  
south Peloponnese (Greece): source models of the 1175  
three strongest events. *Tectonophysics* 471:272–284 1176
- Selby N, Eshun E, Patton H, Douglas A (2005) Un- 1177  
usual long-period Rayleigh wave from a vertical dip- 1178  
slip source: the 7 May 2001, North Sea earthquake. 1179  
*J Geophys Res* 110:B10304. doi:10.1029/2005JB003721 1180
- Sokos E, Serpetsidaki A, Tselentis GA, Zahradnik J (2008) 1181  
Quick assessment of the fault plane, for the recent 1182  
strike-slip event in the North-Western Peloponnese, 1183  
Greece, (8 June 2008, Mw 6.3). EMSC-CSEM Report 1184
- Spudich P, Frazer LN (1984) Use of ray theory to calcu- 1185  
late high-frequency radiation from earthquake sources 1186  
having spatially variable rupture velocity and stress 1187  
drop. *Bull Seismol Soc Am* 74:2061–2082 1188
- Underhill JR (1999) Late Cenozoic deformation of the 1189  
Hellenide forelands, Western Greece. *Geol Soc Am* 1190  
*Bull* 101:613–634 1191
- Vallée M (2007) Rupture properties of the giant suma- 1192  
tra earthquake imaged by empirical Green's function 1193  
analysis. *Bull Seismol Soc Am* 97:103–114 1194
- Vallée M, Bouchon M (2004) Imaging coseismic rupture in 1195  
the far field by slip patches. *Geophys J Int* 156:615–630 1196
- Velasco AA, Ammon CJ, Lay T (1994) Empirical green 1197  
function deconvolution of broadband surface waves: 1198  
Rupture directivity of the 1992 Landers, California 1199  
(Mw = 7.3), earthquake. *Bull Seismol Soc Am* 84:735– 1200  
750 1201
- Velasco AA, Ammon CJ, Farrell J, Pankow K (2004) 1202  
Rupture directivity of the 3 November 2002 denali 1203  
fault earthquake determined from surface waves. *Bull* 1204  
*Seismol Soc Am* 94:293–299 1205
- Warren LM, Shearer PM (2006) Systematic determination 1206  
of earthquake rupture directivity and fault planes from 1207  
analysis of long-period P-wave spectra. *Geophys J Int* 1208  
164:46–62 1209
- Wells DL, Coppersmith KJ (1994) New empirical relations 1210  
among magnitude, rupture length, rupture width, rup- 1211  
ture area and surface displacements. *Bull Seismol Soc* 1212  
*Am* 84:974–1002 1213
- Wessel P, Smith WHF (1998) New improved version of 1214  
the generic mapping tools released. *Eos Trans AGU* 1215  
79:579 1216
- Zahradnik J, Galovic F, Sokos E, Serpetsidaki A, 1217  
Tselentis GA (2008) Quick fault-plane identification 1218  
by geometrical method: application to Mw 6.2 Leoni- 1219  
dio earthquake, January 6, 2008, Greece. *Seismol Res* 1220  
*Lett* 79:653–662 1221

## AUTHOR QUERY

**NO QUERY**

UNCORRECTED PROOF